OXFORD

*Cerebral Cortex*, 2023, **33**, 3562–3574
https://doi.org/10.1093/cercor/bhac292
Advance access publication date 10 August 2022
Original Article

# Normative quantitative relaxation atlases for characterization of cortical regions using magnetic resonance fingerprinting

Joon Yul Choi[1], Siyuan Hu[2], Ting-Yu Su[1,2], Hiroatsu Murakami[1], Yingying Tang[1,3], Ingmar Blümcke[1,4], Imad Najm[1], Ken Sakaie[5], Stephen Jones[5], Mark Griswold[6], Zhong Irene Wang[1,*], Dan Ma[2,*]

[1]Charles Shor Epilepsy Center, Neurological Institute, Cleveland Clinic, 9500 Euclid Ave, Cleveland, OH 44106, United States,
[2]Department of Biomedical Engineering, Case Western Reserve University, 10900 Euclid Ave, Cleveland, OH 44106, United States,
[3]Department of Neurology, West China Hospital of Sichuan University, 37 Guoxue Ln, Wuhou District, Chengdu, Sichuan 610041, China,
[4]Imaging Institute, Cleveland Clinic, 1950 E 89th St U Bldg, Cleveland, OH 44195, United States,
[5]Department of Neuropathology, University of Erlangen, Schlobplatz 4, Erlangen 91054, Germany,
[6]Department of Radiology, Case Western Reserve University, 11100 Euclid Ave, Cleveland, OH 44106, United States

*Corresponding authors: Zhong Irene Wang, PhD, Epilepsy Center, Cleveland Clinic, Desk S-51, 9500 Euclid Avenue, Cleveland OH 44195, United States. Email: wangi2@ccf.org; Dan Ma, PhD, Department of Biomedical Engineering, Case Western Reserve University, B110 Bolwell Building, 11100 Euclid Avenue, Cleveland, OH 44106, United States. Email: dxm302@case.edu

Quantitative magnetic resonance (MR) has been used to study cyto- and myelo-architecture of the human brain non-invasively. However, analyzing brain cortex using high-resolution quantitative MR acquisition can be challenging to perform using 3T clinical scanners. MR fingerprinting (MRF) is a highly efficient and clinically feasible quantitative MR technique that simultaneously provides $T_1$ and $T_2$ relaxation maps. Using 3D MRF from 40 healthy subjects (mean age = 25.6 ± 4.3 years) scanned on 3T magnetic resonance imaging, we generated whole-brain gyral-based normative MR relaxation atlases and investigated cortical-region-based $T_1$ and $T_2$ variations. Gender and age dependency of $T_1$ and $T_2$ variations were additionally analyzed. The coefficient of variation of $T_1$ and $T_2$ for each cortical-region was 3.5% and 7.3%, respectively, supporting low variability of MRF measurements across subjects. Significant differences in $T_1$ and $T_2$ were identified among 34 brain regions ($P < 0.001$), lower in the precentral, postcentral, paracentral lobule, transverse temporal, lateral occipital, and cingulate areas, which contain sensorimotor, auditory, visual, and limbic functions. Significant correlations were identified between age and $T_1$ and $T_2$ values. This study established whole-brain MRF $T_1$ and $T_2$ atlases of healthy subjects using a clinical 3T scanner, which can provide a quantitative and region-specific baseline for future brain studies and pathology detection.

*Key words*: MR fingerprinting; T1 relaxation time; T2 relaxation time; human brain atlas; quantitative MRI.

## Introduction

It is well recognized that cortical gray matter (GM) has varying cyto- and myelo-architecture in different brain areas, with many of these variations related to brain function (Ribas 2010; Amunts and Zilles 2015). Gyral microstructural changes have also been associated with neurological diseases and alterations in cortical functions. Frontal lobe atrophy was correlated with impaired executive function in patients with Parkinson's disease (Lee et al. 2014; Chung et al. 2019). Patients with Alzheimer's disease showed a wide spectrum of GM atrophy in the temporal lobes, precuneus, cingulate gyrus, and inferior frontal cortex (Möller et al. 2013). Cortical atrophy that extends beyond the epileptic cortical lesion was shown in patients with focal epilepsies (Bernasconi et al. 2011; Barkovich et al. 2012; Adler et al. 2017). More recently, regional GM changes in the frontal lobes were also reported in patients with various psychiatric disorders such as schizophrenia, bipolar disorder, and major depressive disorder (Sasabayashi et al. 2021). As there are regional differences in the cyto-architecture of the normal brain cortex, characterizing normal variations of image features in the brain cortex is needed for better identification of region-specific pathological changes from various neurological disorders.

Although magnetic resonance imaging (MRI) has been widely used to investigate tissue changes in the brain non-invasively, conventional MRI techniques have several limitations. First, the conventional $T_1$ weighted ($T_{1w}$) and $T_2$ weighted ($T_{2w}$) images only provide relative contrasts among different tissue types in the brain. Quantitative measurements carried out in the literature were largely limited to morphometric analysis (such as volume, shape, and texture), but not for signal. Although image contrast variations may be visually observed in some of the cortical regions on conventional qualitative MRI, "quantitative" image markers were typically not available to measure the varying cyto- or

**Received:** May 4, 2022. **Revised:** July 4, 2022. **Accepted:** July 5, 2022

myelo- architectures in cortical regions. Second, for normal brain characterization or group-based disease characterization, a large sample size and a reproducible measurement technique are both critical for establishing region-specific baseline and detection of pathological tissue changes. However, $T_{1w}$ and $T_{2w}$ images are influenced by many factors such as pulse sequence types, acquisition sequence parameters, receive coil sensitivity, and geometry and hardware conditions, causing low reproducibility (Bloem et al. 2018). Third, cortical GM is a thin and complex structure with an average thickness of 2.5 mm (Hutton et al. 2008). MRI techniques need to be equipped with high-resolution and large volume coverage to provide the details of whole-brain GM regions. Finally, because of the limited sensitivity of a single contrast-weighted MR image to cortical GM, images from different contrasts are typically analyzed jointly. When different scans from the same subject are processed, subject motion and differences in image resolution and acquisition plane may introduce inherent registration errors, which further reduces the sensitivity of characterizing subtle tissue variations of cortical GM.

Magnetic resonance fingerprinting (MRF) is a novel MRI technique that generates quantitative $T_1$ and $T_2$ maps simultaneously from a single scan (Ma et al. 2013). Compared with conventional MRI scans with weighted contrasts, MRF is much less sensitive to scan settings and scanner variations, leading to high reproducibility that has been validated by multiple studies (Buonincontri et al. 2019; Körzdörfer et al. 2019; Fujita et al. 2021). Compared with other quantitative MRI techniques such as QRAPMASTER, repeatability of MRF was 1.4 and 1.2 times higher on 1.5T and 3.0T MRI, while being 4.8 times faster (Nunez-Gonzalez et al. 2021). MRF has been applied in various clinical studies, demonstrating high sensitivity and specificity to pathological changes due to epilepsy lesions, brain tumors, and prostate tumors (Badve et al. 2015, 2017; Yu et al. 2017; Liao et al. 2018; Ma et al. 2019). An additional advantage of MRF is the absence of image-to-image registration errors, because of the perfectly co-registered quantitative $T_1$ and $T_2$ maps generated by the same scan. The recently developed high-resolution 3D MRF technique was able to provide whole-brain $T_1$ and $T_2$ maps with 1.0-mm$^3$ isotropic resolution from 3T MRI (Ma et al. 2019). These advantages make MRF a promising noninvasive imaging tool for the detailed investigation of whole-brain regions.

In this study, we aimed to develop normative quantitative atlases of gyral-based cortical brain regions using whole-brain MRF $T_1$ and $T_2$ tissue property maps. Specifically, we estimated $T_1$ and $T_2$ values in a total of 68 cortical GM and adjacent white matter (WM) brain regions from 40 healthy adult subjects, in order to establish a quantitative and region-specific baseline. Previous studies have used quantitative imaging to characterize cortical regions (Cohen-Adad et al. 2012; Haast et al. 2016; Marques et al. 2017); however, these studies were typically performed using ultra-high-field 7T MRI. Because quantitative relaxation times (such as $T_1$, $T_2$, and $T_2$*) are field-dependent, the results cannot be directly used as a 3T normative atlas, or as a quantitative baseline for lesion detection for patient scans acquired using 3T clinical systems. To fill this gap, our study constructed a quantitative normative relaxation atlases based on MRF acquired from a 3T clinical scanner. In addition, the multiparametric 3D MRF sequence with 1-mm$^3$ isotropic resolution employed in this study made it possible to simultaneously measure $T_1$ and $T_2$ values at a high-resolution, whereas a previous study utilized separate $T_1$ and $T_2$ mapping sequences with anisotropic resolution (Piredda et al. 2020). We investigated differences in MRF $T_1$ and $T_2$ values for all gyri, with a particular focus on cortical regions containing primary functions, such as the sensorimotor, auditory, and visual cortices. We additionally assessed the correlation of the $T_1$ and $T_2$ values of cortical GM and its adjacent WM. To focus our analysis on the cortical-region-dependent $T_1$ and $T_2$ variations, we recruited healthy subjects with a narrow age range. However, the age and gender dependency of the $T_1$ and $T_2$ values in each region were also analyzed.

## Materials and methods

### MRI acquisition

This study was approved by Institutional Review Board of Cleveland Clinic and all subjects gave written informed consent prior to the MRF scan. We included 40 healthy volunteers (18 men and 22 women; mean age = 25.6 ± 4.3 years; 35 right-handed and 5 left-handed). Healthy volunteers did not have prior history of neurological disorders; both gender and all ethnicity were recruited. MRI scans were performed at a 3T Siemens Prisma scanner with a 20-channel head coil (Erlangen, Germany). A board-certified radiologist (SEJ) reviewed the scans and confirmed the MRIs were normal from all healthy volunteers. The study design is a cross-sectional study and subjects were scanned at one time point.

3D whole-brain MRF was acquired for all participants (field of view (FOV) = 300 × 300 × 144 mm$^3$, 1.0-mm$^3$ isotropic voxels, axial acquisition, scan time = 10 min 24 s; Ma et al. 2013, 2018, 2019). The 3D MRF sequence was based on steady-state precession (FISP) readout with a stack of spirals k-space trajectory (Ma et al. 2018). In addition to the MRF sequence, a 3D $B_1$ mapping sequence was acquired with the same FOV as the MRF to correct for $B_1$ inhomogeneity in the MRF results (scan time = 1 min 50 s; Ma et al. 2018). As reported previously, MRF provides higher motion robustness than conventional MRI scans (Cruz et al. 2019). Furthermore, pads were positioned beside the subject's head to add comfort and minimize movement.

MRF reconstruction was performed using a low-rank model-based algorithm (Ma et al. 2019). A dictionary was generated to contain signal evolutions from a wide range of combinations of $T_1$ (range: 2–3,000 ms) and $T_2$ (range: 3–2,000 ms) using Block Equation. The inner product between the acquired signal and each combination from

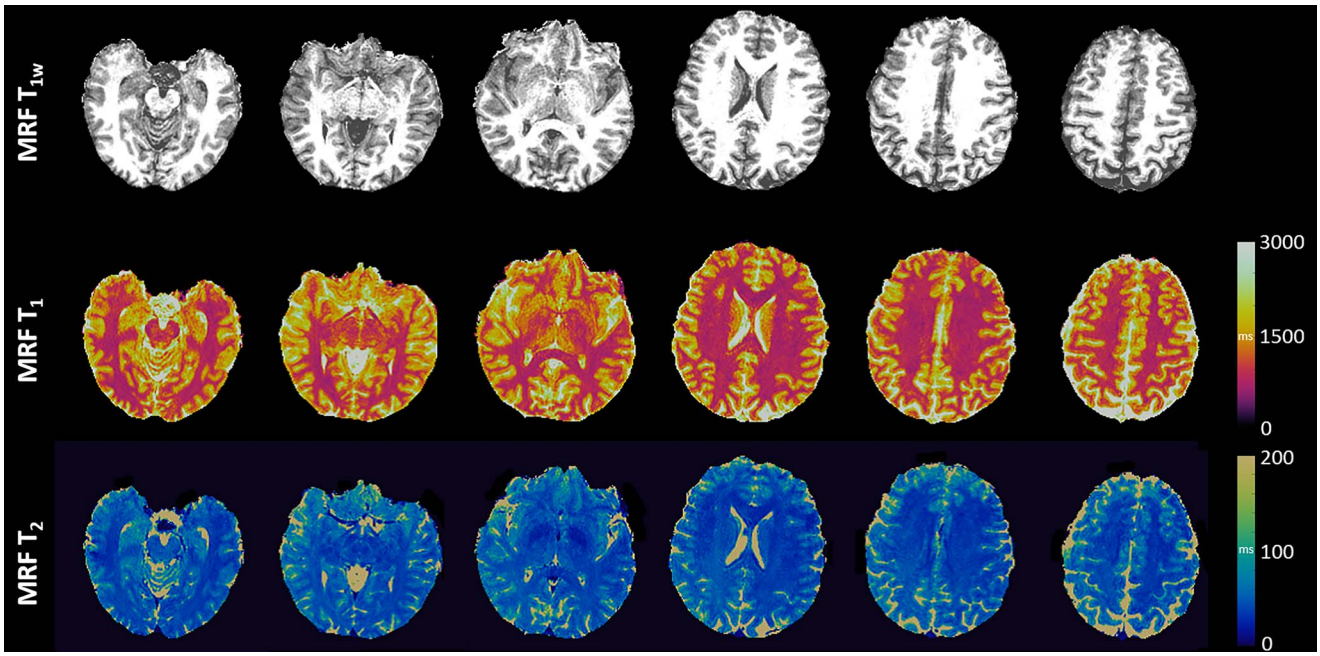


**Fig. 1.** Representative MRF $T_{1w}$, $T_1$, and $T_2$ maps.

the dictionary was performed at each voxel. Then, $T_1$ and $T_2$ values of each voxel were identified using the maximum inner product (Ma et al. 2019). The reconstruction of MRF took 2.7 h on a standalone PC. MRF $T_{1w}$ maps were then synthesized from the $T_1$ maps. Representative MRF $T_{1w}$, $T_1$, and $T_2$ maps are shown in Fig. 1. The MRF maps were reviewed by a board-certified neuroradiologist (SEJ) for image quality and incidental findings, confirming that there were no severe motion artifacts.

For each subject, conventional 3D $T_{1w}$ magnetization-prepared rapid acquisition with gradient echo ($T_{1w}$ Magnetization-prepared rapid gradient-echo (MPRAGE)) images were additionally acquired (FOV = 240 × 240 $mm^2$, matrix = 240 × 240 $mm^2$, thickness = 0.94 mm, resolution = 0.5 × 0.5 × 0.94 $mm^3$, interpolation ON, repetition time = 1,900 ms, echo time = 2.57 ms, inversion time = 1,100 ms, number of slices = 192, flip angle = 10°, GRAPPA = 2, and scan time = 3 min 59 s).

## Data processing for normative quantitative relaxation atlases

The brain segmentation of each subject was performed in Freesurfer with "recon-all" (Dale et al. 1999; Fischl 2012) using the conventional $T_{1w}$ MPRAGE. We utilized the Desikan–Killiany atlas to provide parcellated segmentation of gyral-based cortical GM and adjacent WM (Desikan et al. 2006). The parcellations included 34 different brain structures for each hemisphere (68 regions in total), as listed in Table 1. The gyral-based segmentation masks for GM and adjacent WM are shown in Fig. 2. For the quality control of segmentation, we followed enhancing neuro imaging genetics through meta-analysis (ENIGMA) protocols (Whelan et al. 2018).

To develop normative MRF $T_1$ and $T_2$ atlases for each segmented brain region, we first performed skull stripping for MRF maps, combining MRF $T_{1w}$ and $T_1$ maps to improve the accuracy of skull stripping in the frontal and occipital brain regions using FMRIB Software Library (FSL) (Smith 2002). The MRF $T_{1w}$ maps were then registered to the $T_{1w}$ MPRAGE images using SyN in Advanced Normalization Tools (ANTS) (Avants and Gee 2004). The warping information was directly applied to the $T_1$ and $T_2$ maps to register to the $T_{1w}$ MPRAGE images. Cerebrospinal fluid (CSF) masks were segmented from the registered MRF $T_{1w}$ maps using FSL (Zhang et al. 2001). To minimize partial volume effects from CSF, we excluded voxels with probability of CSF > 10%. Finally, to generate normative $T_1$ and $T_2$ relaxation atlases, $T_1$ and $T_2$ values for a given gyral-based brain structure were averaged across 40 subjects.

## Surface projection of MRF $T_1$ and $T_2$

MRF $T_1$ and $T_2$ surface projections were generated for visualization of the signal variations using all 40 healthy subjects. After skull stripping for all the MRF maps aforementioned, we first generated a MRF $T_{1w}$ template using "antsMultivariateTemplateConstruction2" in ANTs (Avants et al. 2011). Then, warping information obtained from the processing of the MRF $T_{1w}$ template was applied to individual MRF $T_1$ and $T_2$ maps to generate $T_1$ and $T_2$ templates using SyN in ANTs (Avants and Gee 2004). The co-registered $T_1$ and $T_2$ templates were mapped onto the surface template in the MNI152 standard space using computational anatomy toolbox (CAT12; Dahnke et al. 2013), an extension to SPM 12 (Penny et al. 2011) in MATLAB R2021b (MathWorks, Natick, MA). Whole-brain MRF $T_1$ and $T_2$ values were projected on the surface, based on the average value between the GM/CSF border and GM/WM border.

**Table 1.** Labels for brain regions and mean MRF $T_1$ and $T_2$ values of GM and WM adjacent to the cortex.

| Number | Brain region | $T_1$ GM (ms) | $T_2$ GM (ms) | $T_1$ WM (ms) | $T_2$ WM (ms) |
|---|---|---|---|---|---|
| 1 | Bankssts | 1,389 ± 45 | 56.5 ± 2.4 | 866 ± 31 | 41.4 ± 1.5 |
| 2 | Caudal anterior cingulate | 1,341 ± 51 | 55.3 ± 4.6 | 832 ± 35 | 38.4 ± 3.7 |
| 3 | Caudal middle frontal | 1,359 ± 48 | 58.9 ± 4.8 | 867 ± 32 | 42.2 ± 2.1 |
| 4 | Cuneus | 1,384 ± 44 | 56.9 ± 3.1 | 890 ± 35 | 44.2 ± 2.0 |
| 5 | Entorhinal | 1,490 ± 45 | 67.6 ± 8.6 | 963 ± 36 | 46.3 ± 4.4 |
| 6 | Fusiform | 1,433 ± 50 | 62.8 ± 4.6 | 872 ± 32 | 42.6 ± 2.0 |
| 7 | Inferior parietal | 1,368 ± 49 | 58.6 ± 3.0 | 865 ± 32 | 42.8 ± 1.9 |
| 8 | Inferior temporal | 1,459 ± 54 | 66.8 ± 6.3 | 891 ± 36 | 42.4 ± 2.3 |
| 9 | Isthmus cingulate | 1,363 ± 52 | 51.6 ± 3.0 | 849 ± 37 | 39.1 ± 2.5 |
| 10 | Lateral occipital | 1,383 ± 46 | 54.2 ± 3.8 | 878 ± 31 | 42.5 ± 2.4 |
| 11 | Lateral orbitofrontal | 1,409 ± 52 | 66.6 ± 4.6 | 860 ± 35 | 43.6 ± 2.6 |
| 12 | Lingual | 1,412 ± 46 | 55.0 ± 3.1 | 882 ± 34 | 42.9 ± 2.5 |
| 13 | Medial orbitofrontal | 1,393 ± 57 | 66.0 ± 4.9 | 853 ± 36 | 42.5 ± 3.4 |
| 14 | Middle temporal | 1,449 ± 53 | 62.5 ± 3.5 | 894 ± 36 | 41.6 ± 2.0 |
| 15 | Parahippocampal | 1,443 ± 53 | 63.2 ± 5.7 | 912 ± 34 | 43.6 ± 3.1 |
| 16 | Paracentral | 1,335 ± 52 | 58.6 ± 6.6 | 861 ± 32 | 44.9 ± 3.7 |
| 17 | Pars opercularis | 1,397 ± 45 | 58.8 ± 2.7 | 867 ± 30 | 40.4 ± 1.8 |
| 18 | Pars orbitalis | 1,395 ± 50 | 68.1 ± 5.2 | 886 ± 38 | 45.9 ± 3.2 |
| 19 | Pars triangularis | 1,393 ± 46 | 61.6 ± 3.1 | 869 ± 32 | 42.5 ± 2.1 |
| 20 | Pericalcarine | 1,410 ± 49 | 58.5 ± 3.8 | 895 ± 32 | 45.8 ± 2.2 |
| 21 | Postcentral | 1,367 ± 47 | 60.3 ± 4.4 | 883 ± 31 | 44.5 ± 2.6 |
| 22 | Posterior cingulate | 1,353 ± 50 | 53.0 ± 3.1 | 852 ± 35 | 39.6 ± 2.9 |
| 23 | Precentral | 1,357 ± 45 | 59.7 ± 4.7 | 875 ± 31 | 44.9 ± 2.6 |
| 24 | Precuneus | 1,380 ± 48 | 56.3 ± 3.2 | 861 ± 31 | 42.3 ± 2.1 |
| 25 | Rostral anterior cingulate | 1,339 ± 48 | 58.6 ± 4.4 | 821 ± 31 | 39.0 ± 3.1 |
| 26 | Rostral middle frontal | 1,366 ± 48 | 62.0 ± 3.6 | 857 ± 32 | 41.6 ± 2.2 |
| 27 | Superior frontal | 1,381 ± 50 | 64.3 ± 7.3 | 867 ± 33 | 43.6 ± 2.7 |
| 28 | Superior parietal | 1,376 ± 49 | 60.4 ± 5.2 | 871 ± 33 | 44.1 ± 2.5 |
| 29 | Superior temporal | 1,447 ± 46 | 61.7 ± 3.1 | 899 ± 33 | 42.4 ± 2.0 |
| 30 | Supramarginal | 1,381 ± 45 | 57.7 ± 2.8 | 863 ± 32 | 41.0 ± 1.8 |
| 31 | Frontal pole | 1,383 ± 63 | 73.0 ± 12.0 | 902 ± 43 | 47.6 ± 7.7 |
| 32 | Temporal pole | 1,522 ± 52 | 71.2 ± 6.2 | 981 ± 41 | 46.5 ± 3.6 |
| 33 | Transverse temporal | 1,336 ± 41 | 51.4 ± 2.3 | 887 ± 30 | 41.5 ± 1.8 |
| 34 | Insula | 1,424 ± 41 | 60.1 ± 2.9 | 880 ± 25 | 41.8 ± 1.7 |

GM: gray matter, WM: white matter, Bankssts: banks of superior temporal. MRF $T_1$ and $T_2$ values were averaged from right and left hemispheres for each brain region.

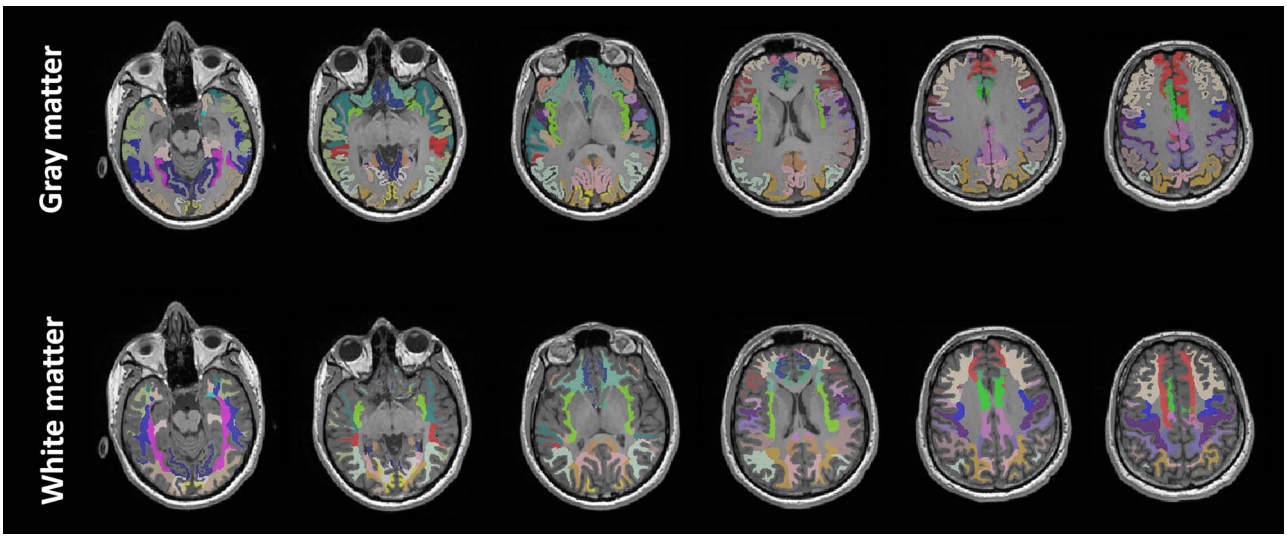


**Fig. 2.** The brain segmentation masks for gyral-based cortical gray matter and WM adjacent to gray matter used in this study.

## Data analysis

Statistical analyses were performed using the statistics and machine learning toolbox in MATLAB. MRF $T_1$ and $T_2$ values were transformed to the logarithmic scale to reduce possible skewed distribution. A one-way analysis of variance (ANOVA) test was performed to test the significant differences between MRF $T_1$ and $T_2$ values of different cortical GM regions. Post-hoc analysis was

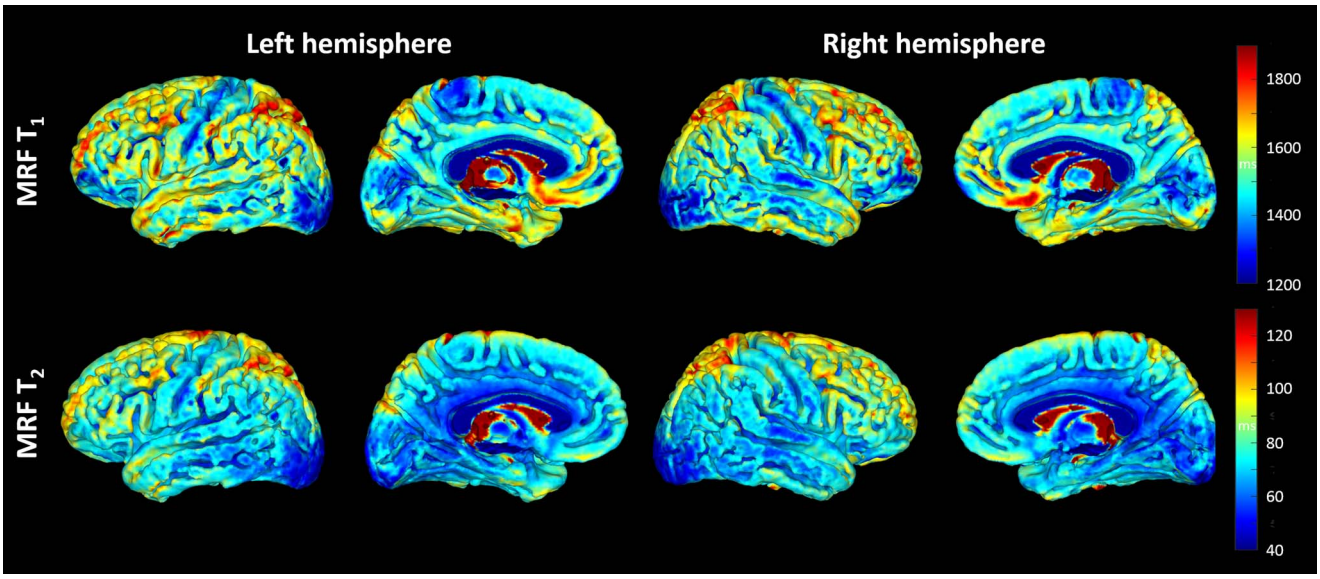


**Fig. 3.** Brain surface projection maps for MRF $T_1$ and $T_2$ of left and right hemispheres.

performed using Tukey's method for multiple comparison correction. The statistical difference between MRF values of male and female was additionally investigated using average $T_1$ and $T_2$ values of both hemispheres.

We performed Spearman's correlation analyses to explore the association between MRF $T_1$ and $T_2$ values in GM and its adjacent WM. Correlation coefficients for variation of different brain regions were calculated using average MRF values across 40 subjects for each region. The association of $T_1$ and $T_2$ values with the age of participants for each region was investigated using average $T_1$ and $T_2$ values of both hemispheres.

## Results

### MRF $T_1$ and $T_2$ surface projections

Average $T_1$ and $T_2$ surface projections of the left and right hemispheres from all subjects are shown in Fig. 3. Visually, low MRF $T_1$ values were seen on the precentral and postcentral gyri (sensorimotor cortex). MRF $T_1$ and $T_2$ values were both low around the posterior superior temporal region (auditory cortex) and lateral/mesial occipital regions (visual cortex). In addition, low $T_1$ values were seen in the paracentral lobule (sensorimotor cortex) and low $T_2$ values in the cingulate.

### MRF $T_1$ and $T_2$ of cortical GM regions

The mean MRF $T_1$ and $T_2$ values in the 34 parcellated brain regions are shown in Table 1. The average coefficient of variations (CV) of the $T_1$ value for 40 subjects in each region were 3.5% and 3.8% for GM and WM, respectively; the average CVs of the $T_2$ value were 7.3% and 6.2% for GM and WM, respectively. Region-based CV values can be found in Supplementary Table 1. The low CV values support low variability of 3D MRF measurement in healthy subjects with similar ages ($25.6 \pm 4.3$ years in our study). The distribution of MRF $T_1$ and $T_2$ values across brain regions was significantly correlated between the left and right hemispheres using Spearman's analysis ($T_1$: rho $= 0.9667$ and $P < 0.001$ in GM, rho $= 0.9016$ and $P < 0.001$ in WM; $T_2$: rho $= 0.9679$ and $P < 0.001$ in GM, rho $= 0.9071$ and $P < 0.001$ in WM), confirming the high similarity of $T_1$ and $T_2$ values between left and right hemispheres. No significant differences between left and right hemispheres were seen for all regions except for 2 (label 33, transverse temporal, for $T_1$ GM; label 24, precuneus, for $T_2$ GM and WM, $P < 0.05$ for all, Bonferroni corrected).

Figure 4 shows box plots of log MRF $T_1$ and $T_2$ values of cortical GM from 34 brain regions (labels corresponding to Table 1). Log MRF $T_1$ and $T_2$ values were significantly different between 34 brain regions in both left and right hemispheres using one-way ANOVA tests ($P < 0.001$). As shown in Fig. 5 and Supplementary Fig. 1, significantly lower MRF $T_1$ values were found in the following regions ($P < 0.05$, Tukey corrected): precentral (label 23, lower than 11/34 regions on left, 12/34 regions on right), postcentral (label 21, lower than 9/34 regions on left, 10/34 regions on right), paracentral (label 16, lower than 24/34 regions on left, 19/34 regions on right), and transverse temporal (label 33, lower than 14/34 regions on left, 26/34 regions on right). On the significantly higher end of MRF $T_1$ values were the following regions ($P < 0.05$, Tukey corrected): temporal pole (label 32, higher than 32/34 regions on left, 32/34 regions on right), entorhinal (label 5, higher than 28/34 regions on left, 30/34 regions on right), inferior temporal (label 8, higher than 27/34 regions on left, 26/34 regions on right), middle temporal (label 14, higher than 26/34 regions on left, 24/34 regions on right), and superior temporal (label 29, higher than 26/34 regions on left, 23/34 regions on right) regions.

As shown in Fig. 6 and Supplementary Fig. 2, significantly lower MRF $T_2$ values were identified in the following regions ($P < 0.05$, Tukey corrected): transverse

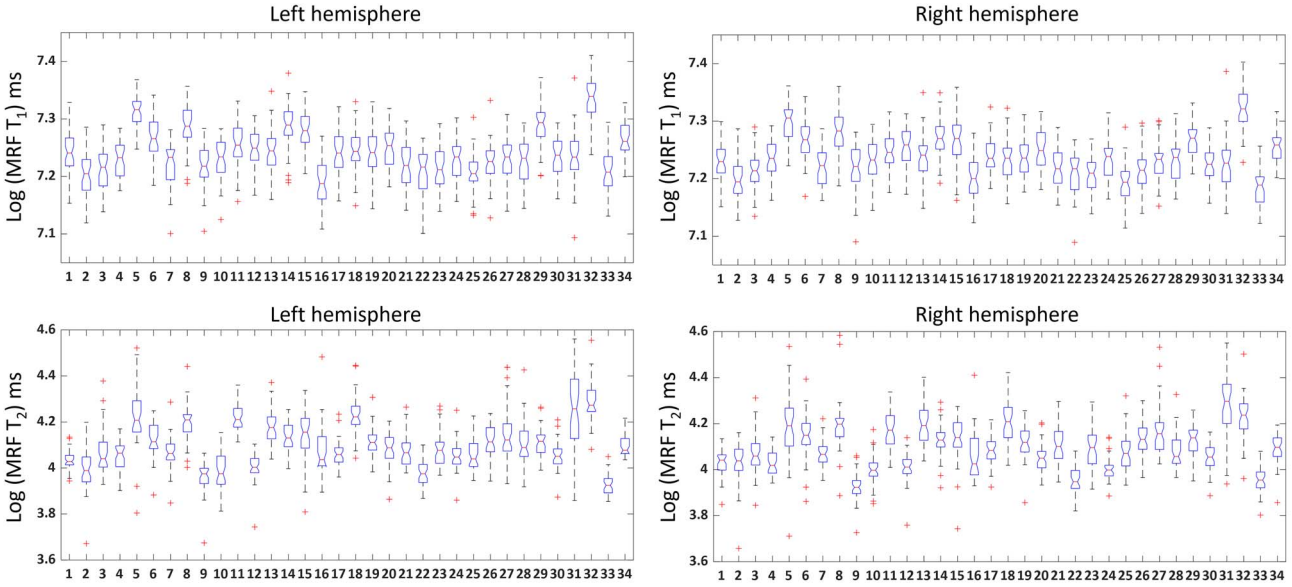


**Fig. 4.** Box plots of log MRF $T_1$ and $T_2$ values of left and right hemispheres. Red line in the box indicates the median value. Asterisk indicates outliers. X-axis consists of 34 labels of the brain mask (labels shown in Table 1). The distribution of MRF $T_1$ and $T_2$ values across brain regions was significantly correlated between the left and right hemispheres using Spearman's analysis ($P < 0.001$).

temporal (label 33, lower than 29/34 regions on left, 28/34 regions on right), lateral occipital (label 10, lower than 27/34 regions on left, 21/34 regions on right), isthmus cingulate (label 9, lower than 28/34 regions on left, 31/34 regions on right), and posterior cingulate (label 22, lower than 27/34 regions on left, 26/34 regions on right). On the significantly higher end of MRF $T_2$ values were the following regions ($P < 0.05$, Tukey corrected): temporal pole (label 32, higher than 32/34 regions on left, 26/34 regions on right), frontal pole (label 31, higher than 29/34 regions on left, 31/34 regions on right), pars orbitalis (label 18, higher than 28/34 regions on left, 25/34 regions on right), lateral orbitofrontal (label 11, higher than 28/34 regions on left, 20/34 regions on right), medial orbitofrontal (label 13, higher than 22/34 regions on left, 21/34 regions on right), and entorhinal (label 5, higher than 28/34 regions on left, 22/34 regions on right) regions. There were no significant gender differences in $T_1$ and $T_2$ values across brain regions ($P > 0.05$, False discovery rate (FDR) corrected).

## Correlation analyses for MRF $T_1$ and $T_2$

We found a significant correlation between MRF $T_1$ in the GM and adjacent WM across all the brain regions (rho = 0.6611, $P < 0.001$). Similarly, MRF $T_2$ also showed significant correlation between GM and adjacent WM (rho = 0.5572, $P < 0.001$). Across all subjects, $T_1$ and $T_2$ values were significantly correlated only in some (but not all) of brain regions (GM, 11 out of 68 regions; WM, 15 out of 68 regions), suggesting that $T_1$ and $T_2$ carry different tissue property information.

Significant negative correlations were found between MRF values and age in many GM regions, as shown in Figs 7 and 8. Namely, caudal middle frontal (label 3), cuneus (label 4), inferior parietal (label 7), isthmus cingulate (label 9), lateral orbitofrontal (label 11), paracentral (label 16), pars opercularis (label 17), pars orbitalis (label 18), pars triangularis (label 19), pericalcarine (label 20), postcentral (label 21), precentral (label 23), precuneus (label 24), rostral middle frontal (label 26), superior frontal (label 27), superior parietal (label 28), supramarginal (label 30), and insula (label 34) regions were significantly correlated with MRF $T_1$ values ($P < 0.05$, Fig. 7). Banks of superior temporal (label 1), caudal middle frontal (label 3), medial orbitofrontal (label 13), pars orbitalis (label 17), pars triangularis (label 19), precentral (label 23), rostral anterior cingulate (label 25), rostral middle frontal (label 26), superior frontal (label 27), superior temporal (label 29), frontal pole (label 31), and transverse temporal (label 33) regions were significantly correlated with MRF $T_2$ ($P < 0.05$, Fig. 8). Note that, although significant negative correlations were identified, CV of the $T_1$ and $T_2$ values in the significant regions were still relatively low for this narrow age range, at $3.5 \pm 0.2\%$ for $T_1$ and $7.1 \pm 3.5\%$ for $T_2$. For the adjacent WM regions, only the frontal pole (label 31, CV = 4.7%) region showed significant correlation between $T_2$ values and age (rho = −0.395, $P = 0.012$).

## Discussion

In this study, we generated normative quantitative $T_1$ and $T_2$ atlases for gyral-based cortical regions using a novel 3D MRF technique. The 1-mm$^3$ isotropic resolution allowed for analysis of GM and adjacent WM regions of the whole-brain with high resolution. The perfectly co-registered $T_1$ and $T_2$ maps from a single MRF scan also enabled the analysis of correlations between

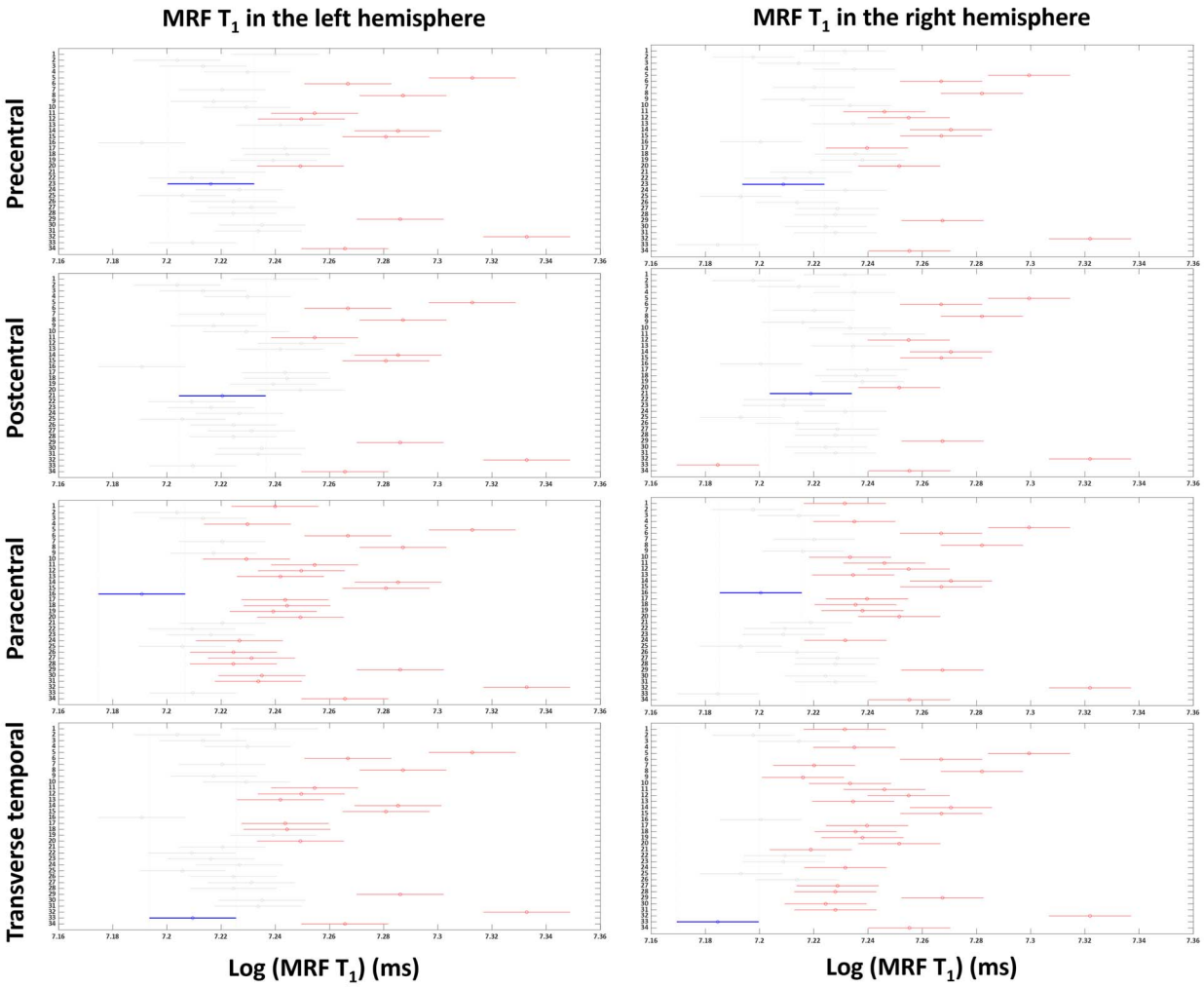


**Fig. 5.** Tukey post-hoc results for MRF $T_1$ values in left and right hemispheres. *X*-axis shows $T_1$ values in a log scale and *Y*-axis shows labels of 34 brain regions (labels shown in Table 1). Red lines indicate the significant areas compared with the area indicated by the blue lines (precentral, postcentral, paracentral, and transverse temporal regions), after Tukey's multiple comparison correction ($P < 0.05$).

different tissue properties. $T_1$ and $T_2$ results from all 68 regions showed low variability across 40 healthy subjects with similar ages, with CV ~3% for $T_1$ and 7% for $T_2$. This low across-subject variability from MRF allowed us to detect subtle differences across normal cortical regions. In addition, as shown in the age-dependency analysis, significant negative correlations between the subjects' age and $T_1$ or $T_2$ values were identified in many of the cortical regions, even within this narrow age range ($25.6 \pm 4.3$ years), suggesting that the 3% and 7% variations in $T_1$ and $T_2$ may even provide physiologically meaningful information related to brain aging. The reliable segmentation of the atlases was shown by the high correlation between MRF values of the left and right hemispheres. The significantly lower-signal regions on $T_1$ and $T_2$ atlases seemed to be consistent with myelin-rich primary functional areas of the brain (e.g. sensory, motor, visual, and auditory cortex). The demonstrated significant correlation between MRF values of cortical GM and those of adjacent WM supported the notion that these regions are structurally and functionally related.

Prior studies showed that $T_1$ was significantly correlated with water mobility (Sigalovsky et al. 2006; Bock et al. 2009; Geyer et al. 2011), myelin (Mottershead et al. 2003; Bot et al. 2004; Schmierer et al. 2004), and extracellular fluid space of tissue (Ormerod et al. 1986). $T_2$ showed significant relationship with water accumulation and gliosis (Kamman et al. 1988) as well as iron accumulation (Desmond et al. 2016). Our results revealed different regions where $T_1$ and $T_2$ showed lower values, potentially reflecting the capability of $T_1$ and $T_2$ to depict the varying cyto- and myelo-architecture changes in a complementary fashion. Correlation analysis between $T_1$ and $T_2$ showed significance only in ~20% of 68 gyral regions, further suggesting that $T_1$ and $T_2$ carry different tissue property information. The higher CV of $T_2$ as compared with $T_1$ could be due to $B_1$ inhomogeneity and magnetization transfer effects (Hilbert et al. 2020). Previous MRF studies have also shown a relatively larger variation

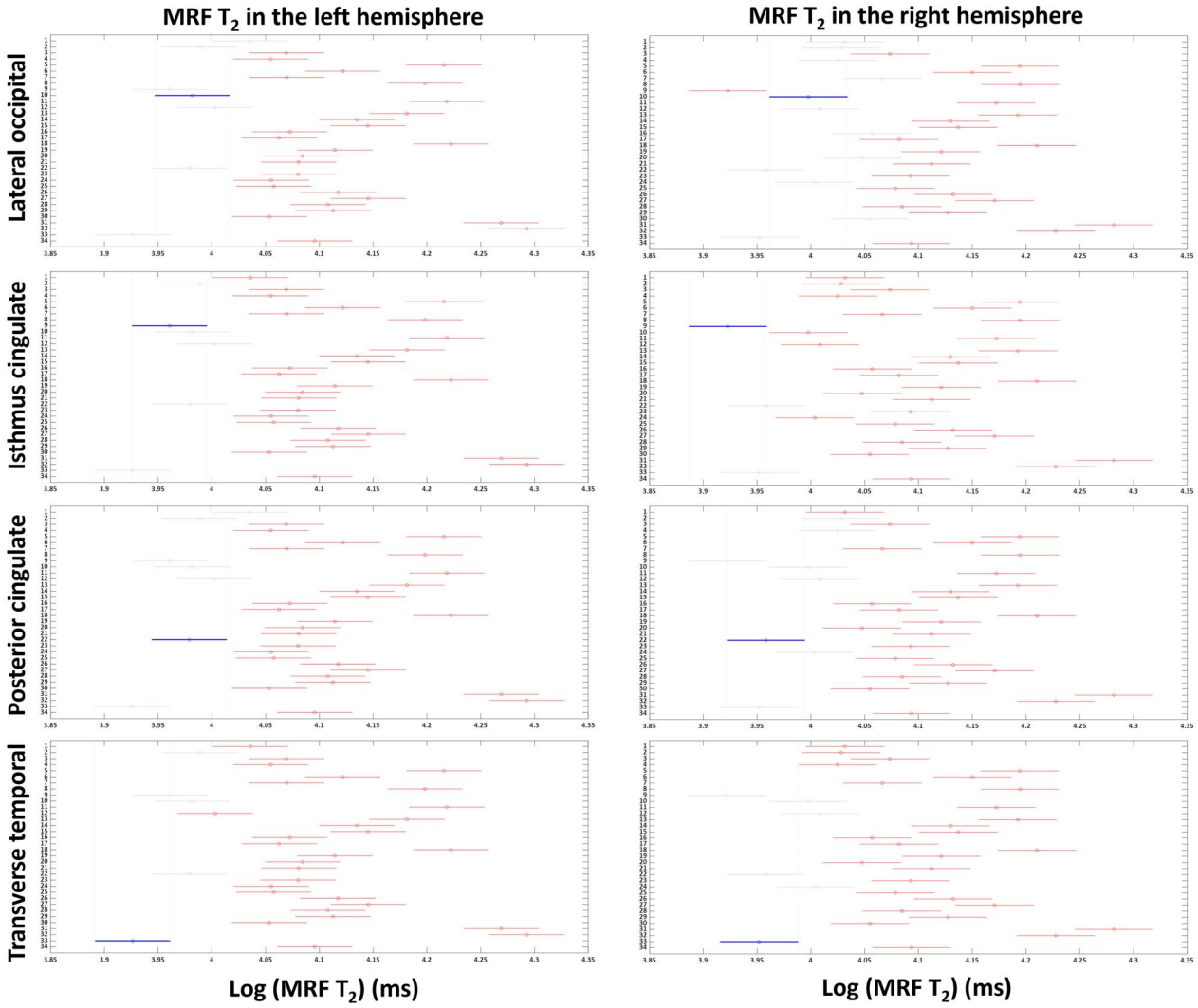


**Fig. 6.** Tukey post-hoc results for MRF $T_2$ values in left and right hemispheres. X-axis shows $T_2$ values in a log scale and Y-axis denotes labels of 34 brain regions (labels shown in Table 1). Red lines indicate the significant areas compared with the area indicated by the blue lines (lateral occipital, isthmus cingulate, posterior cingulate and transverse temporal regions), after Tukey's multiple comparison correction ($P < 0.05$).

of $T_2$ than $T_1$ (Buonincontri et al. 2019; Körzdörfer et al. 2019; Choi et al. 2022).

MRF $T_1$ values were significantly lower in regions carrying primary functions, including precentral and postcentral, transverse temporal, and paracentral regions. Precentral and postcentral gyri are well known to be highly myelinated primary motor and somatosensory cortices (Barbas and García-Cabezas 2015; Rowley et al. 2015). A previous MRI study that used Magnetization-prepared 2 rapid acquisition gradient echo (MP2RAGE) at 7T showed low $T_1$ values in Brodmann areas 1–3 (somatosensory cortices) compared with other Brodmann areas (Marques et al. 2017). The transverse temporal gyri (Heschl's gyri), the most myelinated region in the temporal cortex (Rowley et al. 2015; Gulban et al. 2020), contain primary auditory function. Consistent with our finding, significantly lower $T_1$ values were reported in the transverse temporal region by the aforementioned 7T study (Marques et al. 2017), and myelination-weighted contrast imaging such as $T_{1w}/T_{2w}$* also revealed high signals in this region (Haast et al. 2016). The significantly lower MRF $T_1$ in the paracentral region, a medial continuation of the precentral and postcentral gyri, could also be related to this area being the control hub of motor and sensory innervations (Haines 2017). $T_{1w}/T_{2w}$* myelination-weighted imaging at 7T also showed high level of myelination in this region (Haast et al. 2016).

Carrying complementary tissue property information, MRF $T_2$ data showed different findings than $T_1$ data. Significantly lower $T_2$ was found in the lateral occipital region, which plays an important role in human visual object processing. A prior histology study showed dense myelin staining in the lateral occipital cortex (Ramachandran 2002). Low MRF $T_2$ values in this region may reflect these densely myelinated structures. The lower MRF $T_2$ detected in the cingulate regions is intriguing. The cingulate, being an important part of the

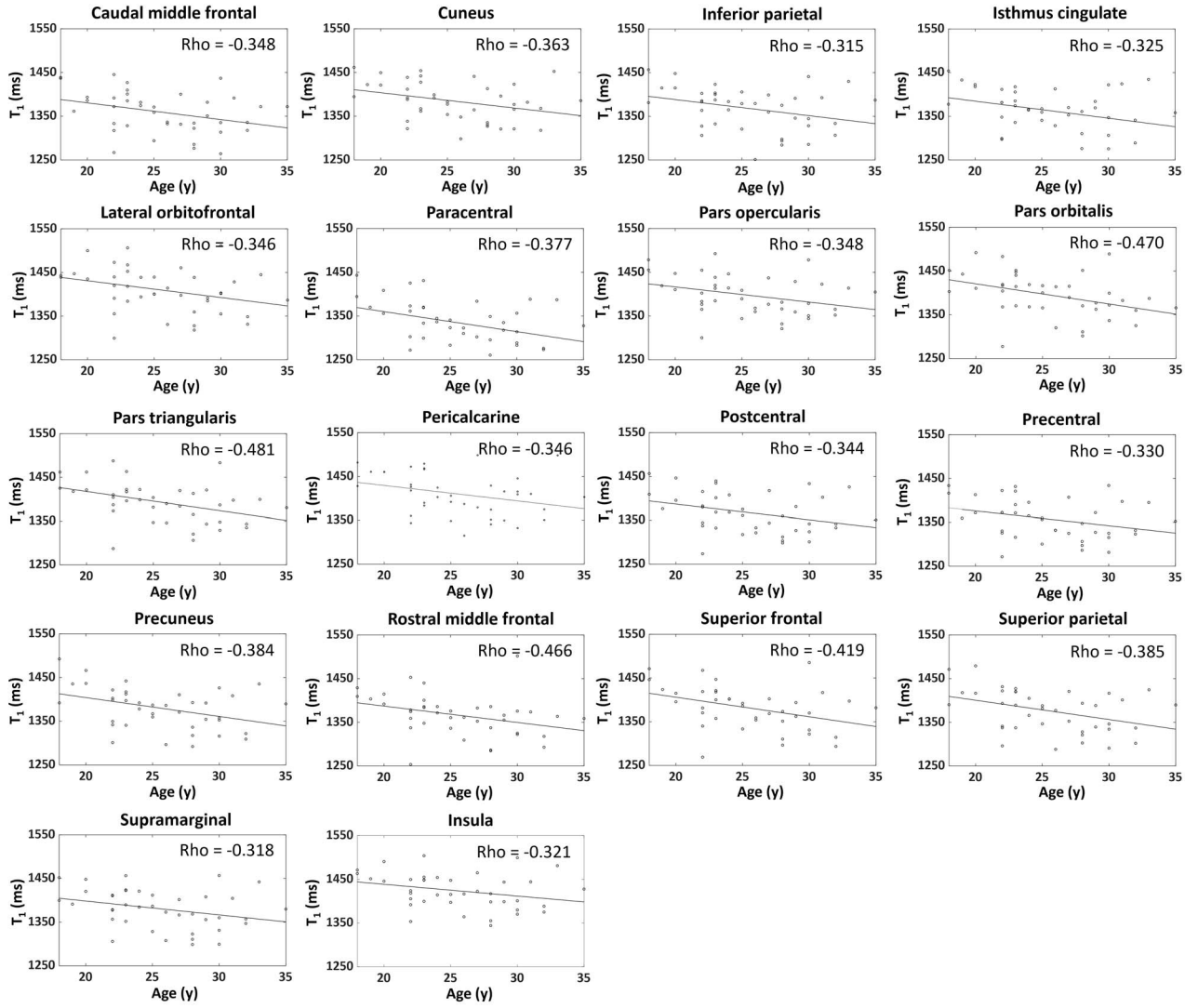


**Fig. 7.** Scatter plots and linear regression lines of $T_1$ values in relation to age for significant regions. Rho values indicate Spearman's correlation ($P < 0.05$).

limbic system, is associated with diverse brain functions and densely interconnected with a variety of other brain regions. Haast et al. reported high levels of myelination in the posterior part of the cingulate cortex by measuring $T_{1w}/T_{2w}$* values (Haast et al. 2016), which is consistent with the low MRF $T_2$ values detected in our study.

The high $T_1$ and $T_2$ values in select brain regions are also interesting to consider. For example, the temporal pole showed high $T_1$ values compared with the other regions, which is consistent with prior studies reporting light myelination in the temporal pole using $T_{1w}/T_{2w}$ imaging (Glasser and Van Essen 2012). High MRF $T_2$ was found in the orbitofrontal regions, which were reported to be extensively involved in emotion and decision-making (Kringelbach 2005). Rolls et al. reported that the orbitofrontal regions had relatively more medium and thin axons and intermediate density of neurons compared with the other regions, which could also be the histological explanation of the $T_2$ variations observed (Rolls 2004).

Intriguingly, our data suggest MRF values of GM are significantly correlated with those of WM adjacent to GM for both $T_1$ and $T_2$. An earlier study demonstrated GM neuro-plasticity was related to brain function (Maguire et al. 2006). Recently, the relationship between neuro-plasticity and brain function was also found in the WM adjacent to GM (Scholz et al. 2010; Zatorre et al. 2012; Douaud et al. 2013). During the visual and motor training, changes in diffusion-tensor imaging were observed in the WM around the intraparietal sulcus (Scholz et al. 2010; Takeuchi et al. 2010; Taubert et al. 2010; Hofstetter et al. 2013; Yotsumoto et al. 2014). Piervincenzi et al. revealed that quadrato motor training resulted in changes in the WM around thalamic radiations, uncinate fasciculi and fronto occipital fasciculi, which were related to sensorimotor and cognitive functions (Piervincenzi et al. 2017). Our study provides further evidence, from the angle of quantitative tissue property measures, to support the notion that WM could be structurally and functionally related to cortical GM. Additional studies

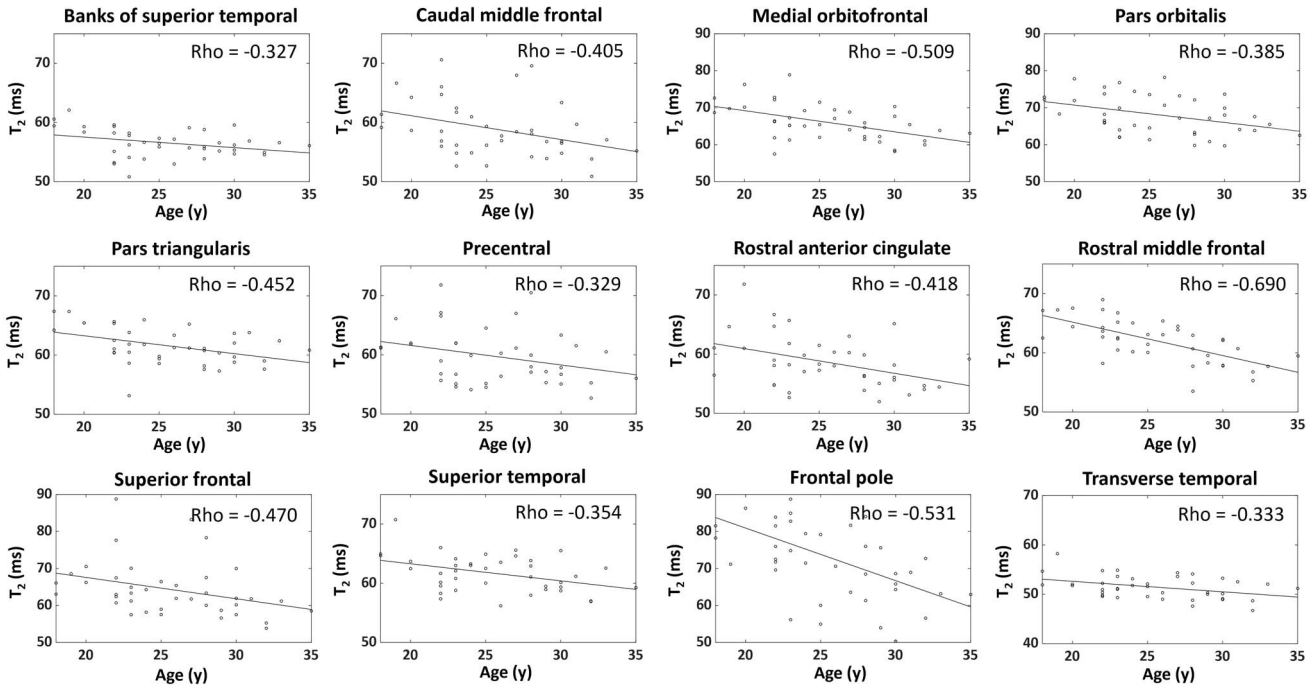


**Fig. 8.** Scatter plots and linear regression lines of $T_2$ values in relation to age for significant regions. Rho values indicate Spearman's correlation ($P < 0.05$).

directly investigating MRF measures and functional measures are needed to further support this point.

The negative correlation between age and MRF $T_1$ or $T_2$ values, within the narrow age range of the recruited subjects ($25.6 \pm 4.3$ years), supports the sensitivity of MRF in measuring microstructural changes in the brain. Hagiwara et al. reported decreases in $T_1$ and $T_2$ values in the brain until 40 years of age, using a multi-echo spin echo sequence for $T_1$ and $T_2$ measurement; a reverse trend of myelin volume fraction in the same subjects supported the $T_1$ and $T_2$ changes (Hagiwara et al. 2021). In another large-cohort study, the myelination pattern of cortical GM in 1,555 healthy subjects was investigated using $T_{1w}/T_{2w}$. A significant linear increase between age and $T_{1w}/T_{2w}$ was detected across 18–35 years of age (Shafee et al. 2015), corroborating our findings. Intriguingly, our data showed only one WM region was significantly correlated between age and MRF values, whereas for cortical GM many regions were significantly correlated. A previous study reported that cortical GM myelination played a dominant role during adolescent development, and was more significantly correlated with age than WM due to different myelination trajectories (Buyanova and Arsalidou 2021). Diffusion-tensor imaging studies also showed relatively stable WM structures during mid-adulthood (Schmithorst et al. 2002; Lebel et al. 2012).

Representing multiparametric imaging characteristics of gyral-based brain regions, the normative quantitative atlases generated in this study have practical clinical significance. The number of subjects in this study ($n = 40$) was larger than previous quantitative relaxation studies, which recruited only 6 (Marques et al. 2017) and 21 (Fujita et al. 2021) healthy subjects to investigate the regional difference between brain regions using quantitative $T_1$ and $T_2$ (or $T_2$*) maps. The high stability of the MRF-based atlases as reported in our study, reflected by a CV of 3% in $T_1$ and 7% in $T_2$, may facilitate the detection of disease-related changes through quantitative comparative analysis. For example, in patients with focal epilepsy, comparing individual patient's images with a normative atlas (based on conventional weighted images) has been frequently performed for lesion detection (Huppertz et al. 2008; House et al. 2013; Wang et al. 2015; David et al. 2021). Current normative atlases were typically generated by $T_{1w}$ and $T_{2w}$ images, so the quantitative comparisons were largely performed by morphometry, which can be inherently limited by lower sensitivity and reproducibility compared with quantitative MRI techniques (Bloem et al. 2018). The normative atlases generated in this study have the potential to address these limitations by providing region-specific and quantitative baselines. Furthermore, the perfectly co-registered $T_1$ and $T_2$ atlases in this study provide complementary, multiparametric information, which can also be essential for the detection of subtle lesional changes associated with neurological diseases that cannot be resolved by one single contrast. The value/necessity of using multiparametric MR comparisons has been illustrated in many prior studies in epilepsy (House et al. 2013; Adler et al. 2017; Hong et al. 2017). Taken together, the MRF $T_1$ and $T_2$ atlases generated in this study have the potential to provide highly sensitive quantitative, region-specific, and multiparametric baselines for the detection of lesional changes associated with neurological diseases.

Although the vast majority of the brain regions did not show significant differences in MRF measures between left and right hemisphere, the transverse temporal region

showed significant differences between left and right for $T_1$ of GM, and the precuneus showed significant differences between left and right for $T_2$ of GM as well as WM. A number of prior studies investigated left and right hemispheric differences in the normal brain. It was reported that the left transverse temporal cortex was more associated with the rate of auditory stimuli, whereas the same region on the right was more related to the spectral characteristics (Warrier et al. 2009). The right transverse temporal cortex was shown to harbor denser and more interconnected columnar structure than the left transverse temporal region (Sigalovsky et al. 2006). These differences may result in the significant hemispheric difference in $T_1$ as measured by MRF. Prior functional imaging studies reported differences of activation patterns between left and right precuneus for highly integrated tasks such as visual–spatial imagery and episodic memory retrieval (Cavanna and Trimble 2006). Further studies are warranted to confirm the hemispheric difference in $T_1$ and $T_2$ in the transverse temporal and precuneus regions, as well as their anatomo-functional underpinnings.

The current study has a few limitations. First, the normative atlases may still contain some potential partial volume effects from CSF. The pericalcarine region, which contains primary visual function, did not show significantly lower $T_1$ and $T_2$ values compared with the other brain regions, which is likely due to this reason. Second, the study focused on the cortical GM and the WM adjacent to the cortex. Analysis for the subcortical regions such as subcortical WM and deep GM using 3D MRF would be informative for future brain normative atlas studies for neurological diseases such as Parkinson's disease and multiple sclerosis. Third, for the purpose of estimating $T_1$ and $T_2$ variations across cortical GM regions on a group level, the atlases were generated using data from young adult subjects with a narrow age range. As can be seen from the results, the quantitative $T_1$ and $T_2$ values were still highly sensitivity to age; therefore, age-dependent or age-modeled atlases are very much needed for future studies. Lastly, although the current study has by far the largest cohort for quantitative MRI studies in the normal brain, the normative database could still benefit from additional subjects; future studies with larger sample size are still needed to confirm our findings.

Using multiparametric normative relaxation atlases generated from quantitative MRF-derived $T_1$ and $T_2$ maps, we can differentiate cortical regions with gyrus-specific differences, especially in the precentral, postcentral, paracentral lobule, transverse temporal, lateral occipital, and cingulate areas, which contain sensorimotor, auditory, visual, and limbic functions. This supports the sensitivity of MRF $T_1$ and $T_2$ to cortical regions with different cyto- or myelo-architectures related to brain functions. The significant correlation between MRF values of GM and adjacent WM may support the notion that they are structurally and functionally related. The normative relaxation atlases generated in this study have the potential to provide quantitative, region-specific, and multiparametric baselines for the detection of pathological changes associated with neurological diseases.

## Supplementary material

Supplementary material is available at *Cerebral Cortex* online.

## Funding

This study was supported by the National Institutes of Health (NIH) [grant numbers R01 NS109439 and R21 EB026764].

*Conflict of interest statement*: Imad Najm is on the Speakers' bureau of Eisai. Stephen Jones received travel and speaker fees from SIEMENS Healthineers. Dan Ma and Mark Griswold have MRF patents licensed by Siemens. Other authors have no competing interests to disclose.

## Data availability

The data that support the findings of this study are available from the corresponding authors (ZIW and DM), upon reasonable request.

## References

Adler S, Lorio S, Jacques TS, Benova B, Gunny R, Cross JH, Baldeweg T, Carmichael DW. Towards in vivo focal cortical dysplasia phenotyping using quantitative MRI. *NeuroImage Clin*. 2017:15:95–105.

Amunts K, Zilles K. Architectonic mapping of the human brain beyond Brodmann. *Neuron*. 2015:88(6):1086–1107.

Avants B, Gee JC. Geodesic estimation for large deformation anatomical shape averaging and interpolation. *NeuroImage*. 2004:23: S139–S150.

Avants BB, Tustison NJ, Song G, Cook PA, Klein A, Gee JC. A reproducible evaluation of ANTs similarity metric performance in brain image registration. *NeuroImage*. 2011:54(3): 2033–2044.

Badve C, Yu A, Rogers M, Ma D, Liu Y, Schluchter M, Sunshine J, Griswold M, Gulani V. Simultaneous T1 and T2 brain relaxometry in asymptomatic volunteers using magnetic resonance fingerprinting. *Tomography*. 2015:1(2):136–144.

Badve C, Yu A, Dastmalchian S, Rogers M, Ma D, Jiang Y, Margevicius S, Pahwa S, LuZ SM, Sunshine J, et al. MR fingerprinting of adult brain tumors: initial experience. *Am J Neuroradiol*. 2017:38(3):492–499.

Barbas H, García-Cabezas M. Motor cortex layer 4: less is more. *Trends Neurosci*. 2015:38(5):259–261.

Barkovich AJ, Guerrini R, Kuzniecky RI, Jackson GD, Dobyns WB. A developmental and genetic classification for malformations of cortical development: Update 2012. *Brain*. 2012:135(5): 1348–1369.

Bernasconi A, Bernasconi N, Bernhardt BC, Bernasconi A, Bernasconi A, Bernasconi N, Bernhardt BC, Schrader D. Advances in MRI for "cryptogenic" epilepsies. *Nat Rev Neurol*. 2011:7(2): 99–108.

Bloem JL, Reijnierse M, Huizinga TWJ, Mil AHMVDH. MR signal intensity : staying on the bright side in MR image interpretation. *Rheum Musculoskelet Dis*. 2018:4(1):e000728.

Bock NA, Kocharyan A, Liu JV, Silva AC. Visualizing the entire cortical myelination pattern in marmosets with magnetic resonance imaging. *J Neurosci Methods*. 2009:185(1):15–22.

Bot JCJ, Blezer ELA, Kamphorst W, Nijeholt GJLÀ, Ader HJ, Castelijns JA, Ig KN, Bergers E, Ravid R, Polman C, et al. The spinal cord in multiple sclerosis: Relationship of high-spatial- resolution quantitative MR imaging findings to histopathologic results. *Radiology*. 2004:233(2):531–540.

Buonincontri G, Biagi L, Retico A, Cecchi P, Cosottini M, Gallagher FA, Gómez PA, Graves MJ, McLean MA, Riemer F, et al. Multi-site repeatability and reproducibility of MR fingerprinting of the healthy brain at 1.5 and 3.0 T. *NeuroImage*. 2019:195:362–372.

Buyanova IS, Arsalidou M. Cerebral white matter myelination and relations to age, gender, and cognition: a selective review. *Front Hum Neurosci*. 2021:15:1–22.

Cavanna AE, Trimble MR. The precuneus: a review of its functional anatomy and behavioural correlates. *Brain*. 2006:129(3):564–583.

Choi JY, Krishnan B, Hu S, Martinez D, Tang Y, Wang X, Sakaie K, Jones S, Murakami H, Blümcke I, et al. Using magnetic resonance fingerprinting to characterize periventricular nodular heterotopias in pharmacoresistant epilepsy. *Epilepsia*. 2022:63(5):1225–1237.

Chung SJ, Yoo HS, Lee YH, Lee HS, Ye BS, Sohn YH, Kwon H, Lee PH. Frontal atrophy as a marker for dementia conversion in Parkinson's disease with mild cognitive impairment. *Hum Brain Mapp*. 2019:40(13):3784–3794.

Cohen-Adad J, Polimeni JR, Helmer KG, Benner T, McNab JA, Wald LL, Rosen BR, Mainero C. T 2∗ mapping and B 0 orientation-dependence at 7T reveal cyto- and myeloarchitecture organization of the human cortex. *NeuroImage*. 2012:60(2):1006–1014.

Cruz G, Jaubert O, Schneider T, Botnar RM, Prieto C. Rigid motion-corrected magnetic resonance fingerprinting. *Magn Reson Med*. 2019:81(2):947–961.

Dahnke R, Yotter RA, Gaser C. Cortical thickness and central surface estimation. *NeuroImage*. 2013:65:336–348.

Dale AM, Fischl B, Sereno MI. Cortical surface-based analysis. *NeuroImage*. 1999:9(2):179–194.

David B, Kröll-Seger J, Schuch F, Wagner J, Wellmer J, Woermann F, Oehl B, Van Paesschen W, Breyer T, Becker A, et al. External validation of automated focal cortical dysplasia detection using morphometric analysis. *Epilepsia*. 2021:62(4):1005–1021.

Desikan RS, Ségonne F, Fischl B, Quinn BT, Dickerson BC, Blacker D, Buckner RL, Dale AM, Maguire RP, Hyman BT, et al. An automated labeling system for subdividing the human cerebral cortex on MRI scans into gyral based regions of interest. *NeuroImage*. 2006:31(3):968–980.

Desmond KL, Al-Ebraheem A, Janik R, Oakden W, Kwiecien JM, Dabrowski W, Rola R, Geraki K, Farquharson MJ, Stanisz GJ, et al. Differences in iron and manganese concentration may confound the measurement of myelin from R1 and R2 relaxation rates in studies of dysmyelination. *NMR Biomed*. 2016:29(7):985–998.

Douaud G, Menke RAL, Gass A, Monsch AU, Rao A, Whitcher B, Zamboni G, Matthews PM, Sollberger M, Smith S. Brain microstructure reveals early abnormalities more than two years prior to clinical progression from mild cognitive impairment to Alzheimer's disease. *J Neurosci*. 2013:33(5):2147–2155.

Fischl B. Free surfer. *NeuroImage*. 2012:62(2):774–781.

Fujita S, Buonincontri G, Cencini M, Fukunaga I, Takei N, Schulte RF, Hagiwara A, Uchida W, Hori M, Kamagata K, et al. Repeatability and reproducibility of human brain morphometry using three-dimensional magnetic resonance fingerprinting. *Hum Brain Mapp*. 2021:42(2):275–285.

Geyer S, Weiss M, Reimann K, Lohmann G, Turner R. Microstructural parcellation of the human cerebral cortex - from Bbrodmann's post-mortem map to in vivo mapping with high-field magnetic resonance imaging. *Front Hum Neurosci*. 2011:5:1–7.

Glasser MF, Van Essen D. Mapping human cortical areas in vivo based on myelin content as revealed by T1- and T2-weighted MRI. *J Neurosci*. 2012:31:11597–11616.

Gulban OF, Goebel R, Moerel M, Zachlod D, Mohlberg H, Amunts K, de Martino F. Improving a probabilistic cytoarchitectonic atlas of auditory cortex using a novel method for inter-individual alignment. *Elife*. 2020:9:1–29.

Haast RAM, Ivanov D, Formisano E, Uludağ K. Reproducibility and reliability of quantitative and weighted T1 and T2∗ mapping for myelin-based cortical parcellation at 7 tesla. *Front Neuroanat*. 2016:10:1–17.

Hagiwara A, Fujimoto K, Kamagata K, Murata S, Irie R, Kaga H, Someya Y, Andica C, Fujita S, Kato S, et al. Age-related changes in relaxation times, proton density, myelin, and tissue volumes in adult brain analyzed by 2-dimensional quantitative synthetic magnetic resonance imaging. *Investig Radiol*. 2021:56(3):163–172.

Haines DE. *Fundamental neuroscience for basic and clinical applications*. 5th ed. Amsterdam: Elsevier Health Sciences; 2017

Hilbert T, Xia D, Block KT, Yu Z, Lattanzi R, Sodickson DK, Kober T, Cloos MA. Magnetization transfer in magnetic resonance fingerprinting. *Magn Reson Med*. 2020:84(1):128–141.

Hofstetter S, Tavor I, Moryosef ST, Assaf Y. Short-term learning induces white matter plasticity in the fornix. *J Neurosci*. 2013:33(31):12844–12850.

Hong S-J, Bernhardt BC, Caldairou B, Hall JA, Guiot MC, Schrader D, Bernasconi N, Bernasconi A. Multimodal MRI profiling of focal cortical dysplasia type II. *Neurology*. 2017:88(8):734–742.

House PM, Lanz M, Holst B, Martens T, Stodieck S, Huppertz HJ. Comparison of morphometric analysis based on T1- and T2-weighted MRI data for visualization of focal cortical dysplasia. *Epilepsy Res*. 2013:106(3):403–409.

Huppertz HJ, Wellmer J, Staack AM, Altenmüller DM, Urbach H, Kröll J, Altenmuller DM, Urbach H, Kroll J. Voxel-based 3D MRI analysis helps to detect subtle forms of subcortical band heterotopia. *Epilepsia*. 2008:49(5):772–785.

Hutton C, DeVita E, Ashburner J, Deichmann R, Turner R. Voxel-based cortical thickness measurements in MRI. *NeuroImage*. 2008:40(4):1701–1710.

Kamman RL, Go KG, Brouwer W, Berendsen HJC. Nuclear magnetic resonance relaxation in experimental brain edema: Effects of water concentration, protein concentration, and temperaturele. *Magn Reson Med*. 1988:6(3):265–274.

Körzdörfer G, Kirsch R, Liu K, Pfeuffer J, Hensel B, Jiang Y, Ma D, Gratz M, Bär P, Bogner W, et al. Reproducibility and repeatability of MR fingerprinting relaxometry in the human brain. *Radiology*. 2019:292(2):429–437.

Kringelbach ML. The human orbitofrontal cortex: linking reward to hedonic experience. *Nat Rev Neurosci*. 2005:6(9):691–702.

Lebel C, Gee M, Camicioli R, Wieler M, Martin W, Beaulieu C. Diffusion tensor imaging of white matter tract evolution over the lifespan. *NeuroImage*. 2012:60(1):340–352.

Lee JE, Cho KH, Song SK, Kim HJ, Lee HS, Sohn YH, Lee PH. Exploratory analysis of neuropsychological and neuroanatomical correlates of progressive mild cognitive impairment in Parkinson's disease. *J Neurol Neurosurg Psychiatry*. 2014:85(1):7–16.

Liao C, Wang K, Cao X, Li Y, Wu D, Ye H, Ding Q, He H, Zhong J. Detection of lesions in mesial temporal lobe epilepsy by using MR fingerprinting. *Radiology*. 2018:288(3):804–812.

Ma D, Gulani V, Seiberlich N, Liu K, Sunshine JL, Duerk JL, Griswold MA. Magnetic resonance fingerprinting. *Nature*. 2013:495(7440):187–192.

Ma D, Jiang Y, Chen Y, Mcgivney D, Mehta B, Gulani V, Griswold M. Fast 3D magnetic resonance fingerprinting for a whole-brain coverage. *Magn Reson Med*. 2018:79(4):2190–2197.

Ma D, Jones SE, Deshmane A, Sakaie K, Pierre EY, Larvie M, Mcgivney D, Blümcke I, Krishnan B, Lowe M, et al. Development of high-resolution 3D MR fingerprinting for detection and characterization of epileptic lesions. *J Magn Reson Imaging*. 2019:49(5):1333–1346.

Maguire EA, Woollett K, Spiers HJ. London taxi drivers and bus drivers: a structural MRI and neuropsychological analysis. *Hippocampus*. 2006:16(12):1091–1101.

Marques JP, Khabipova D, Gruetter R. Studying cyto and myeloarchitecture of the human cortex at ultra-high field with quantitative imaging: R1, R2∗ and magnetic susceptibility. *NeuroImage*. 2017:147:152–163.

Möller C, Vrenken H, Jiskoot L, Versteeg A, Barkhof F, Scheltens P, van derFlier WM. Different patterns of gray matter atrophy in early- and late-onset Alzheimer's disease. *Neurobiol Aging*. 2013:34(8):2014–2022.

Mottershead JP, Schmierer K, Clemence M, Thornton JS, Scaravilli F, Barker GJ, Tofts PS, Newcombe J, Cuzner ML, Ordidge RJ, et al. High field MRI correlates of myelin content and axonal density in multiple sclerosis: A post-mortem study of the spinal cord. *J Neurol*. 2003:250(11):1293–1301.

Nunez-Gonzalez L, Kotek G, Gómez PA, Buonincontri G, Vogel M, Krestin GP, Poot DHJ, Hernandez-Tamames JA. Accuracy and repeatability of QRAPMASTER and MRF-vFA. *Magn Reson Imaging*. 2021:83:196–207.

Ormerod IEC, Bronstein A, Rudge P, Johnson G, Mac Manus D, Halliday AM, Barratt H, DuBoulay EH, Kendal BE, Moseley IF, et al. Magnetic resonance imaging in clinically isolated lesions of the brain stem. *J Neurol Neurosurg Psychiatry*. 1986:49(7):737–743.

Penny WD, Ashuburner JT, Kiebel SJ, Nichols TE. *Statistical parametric mapping: the analysis of functional brain images*. Amsterdam: Elsevier Science; 2011

Piervincenzi C, Ben-Soussan TD, Mauro F, Mallio CA, Errante Y, Quattrocchi CC, Carducci F. White matter microstructural changes following quadrato motor training: A longitudinal study. *Front Hum Neurosci*. 2017:11:1–16.

Piredda GF, Hilbert T, Granziera C, Bonnier G, Meuli R, Molinari F, Thiran JP, Kober T. Quantitative brain relaxation atlases for personalized detection and characterization of brain pathology. *Magn Reson Med*. 2020:83(1):337–351.

Ramachandran VS. *Encyclopedia of the human brain*. San Diego: Academic Press; 2002

Ribas GC. The cerebral sulci and gyri. *Neurosurg Focus*. 2010:28(2).

Rolls ET. The functions of the orbitofrontal cortex. *Brain Cogn*. 2004:55(1):11–29.

Rowley CD, Bazin PL, Tardif CL, Sehmbi M, Hashim E, Zaharieva N, Minuzzi L, Frey BN, Bock NA. Assessing intracortical myelin in the living human brain using myelinated cortical thickness. *Front Neurosci*. 2015:9:1–14.

Sasabayashi D, Takahashi T, Takayanagi Y, Suzuki M. Anomalous brain gyrification patterns in major psychiatric disorders: a systematic review and transdiagnostic integration. *Transl Psychiatry*. 2021:11(1):176.

Schmierer K, Scaravilli F, Altmann DR, Barker GJ, Miller DH. Magnetization transfer ratio and myelin in postmortem multiple sclerosis brain. *Ann Neurol*. 2004:56(3):407–415.

Schmithorst VJ, Wilke M, Dardzinski BJ, Holland SK. Correlation of white matter diffusivity and anisotropy with age during childhood and adolescence: a cross-sectional diffusion-tensor MR imaging study. *Radiology*. 2002:222(1):212–218.

Scholz J, Klein MC, Behrens TEJ, Johansen-berg H. Europe PMC funders group training induces changes in white matter architecture. *Nat Neurosci*. 2010:12(11):1370–1371.

Shafee R, Buckner RL, Fischl B. Gray matter myelination of 1555 human brains using partial volume corrected MRI images. *NeuroImage*. 2015:105:473–485.

Sigalovsky IS, Fischl B, Melcher JR. Mapping an intrinsic MR property of gray matter in auditory cortex of living humans: a possible marker for primary cortex and hemispheric differences. *NeuroImage*. 2006:32(4):1524–1537.

Smith SM. Fast robust automated brain extraction. *Hum Brain Mapp*. 2002:17(3):143–155.

Takeuchi H, Sekiguchi A, Taki Y, Yokoyama S, Yomogida Y, Komuro N, Yamanouchi T, Suzuki S, Kawashima R. Training of working memory impacts structural connectivity. *J Neurosci*. 2010:30(9):3297–3303.

Taubert M, Draganski B, Anwander A, Müller K, Horstmann A, Villringer A, Ragert P. Dynamic properties of human brain structure: learning-related changes in cortical areas and associated fiber connections. *J Neurosci*. 2010:30(35):11670–11677.

Wang ZI, Jones SE, Jaisani Z, Najm IM, Prayson RA, Burgess RC, Krishnan B, Ristic A, Wong CH, Bingaman W, et al. Voxel-based morphometric magnetic resonance imaging (MRI) postprocessing in MRI-negative epilepsies. *Ann Neurol*. 2015:77(6):1060–1075.

Warrier C, Wong P, Penhune V, Zatorre R, Parrish T, Abrams D, Kraus N. Relating structure to function: Heschl's gyrus and acoustic processing. *J Neurosci*. 2009:29(1):61–69.

Whelan CD, Altmann A, Botía JA, Jahanshad N, Hibar DP, Absil J, Alhusaini S, Alvim MKM, Auvinen P, Bartolini E, et al. Structural brain abnormalities in the common epilepsies assessed in a worldwide ENIGMA study. *Brain*. 2018:141(2):391–408.

Yotsumoto Y, Chang LH, Ni R, Pierce R, Andersen GJ, Watanabe T, Sasaki Y. White matter in the older brain is more plastic than in the younger brain. *Nat Commun*. 2014:5(1):5504.

Yu AC, Ponsky LE, Dastmalchian S, Rogers M, Mcgivney D, Griswold MA. Development of a combined MR fingerprinting and diffusion examination for prostate. 2017:283:729–738.

Zatorre RJ, Fields RD, Johansen-Berg H. Plasticity in gray and white: neuroimaging changes in brain structure during learning. *Nat Neurosci*. 2012:15(4):528–536.

Zhang Y, Brady M, Smith S. Segmentation of brain MR images through a hidden Markov random field model and the expectation-maximization algorithm. *IEEE Trans Med Imaging*. 2001:20(1):45–57.